LETTER

doi:10.1038/nature10941

Designer Dirac fermions and topological phases in molecular graphene

Kenjiro K. Gomes[1,2]*, Warren Mar[2,3]*, Wonhee Ko[2,4]*, Francisco Guinea[5] & Hari C. Manoharan[1,2]

The observation of massless Dirac fermions in monolayer graphene has generated a new area of science and technology seeking to harness charge carriers that behave relativistically within solid-state materials[1]. Both massless and massive Dirac fermions have been studied and proposed in a growing class of Dirac materials that includes bilayer graphene, surface states of topological insulators and iron-based high-temperature superconductors. Because the accessibility of this physics is predicated on the synthesis of new materials, the quest for Dirac quasi-particles has expanded to artificial systems such as lattices comprising ultracold atoms[2–4]. Here we report the emergence of Dirac fermions in a fully tunable condensed-matter system—molecular graphene—assembled by atomic manipulation of carbon monoxide molecules over a conventional two-dimensional electron system at a copper surface[5]. Using low-temperature scanning tunnelling microscopy and spectroscopy, we embed the symmetries underlying the two-dimensional Dirac equation into electron lattices, and then visualize and shape the resulting ground states. These experiments show the existence within the system of linearly dispersing, massless quasi-particles accompanied by a density of states characteristic of graphene. We then tune the quantum tunnelling between lattice sites locally to adjust the phase accrual of propagating electrons. Spatial texturing of lattice distortions produces atomically sharp p–n and p–n–p junction devices with two-dimensional control of Dirac fermion density and the power to endow Dirac particles with mass[6–8]. Moreover, we apply scalar and vector potentials locally and globally to engender topologically distinct ground states and, ultimately, embedded gauge fields[9–12], wherein Dirac electrons react to 'pseudo' electric and magnetic fields present in their reference frame but absent from the laboratory frame. We demonstrate that Landau levels created by these gauge fields can be taken to the relativistic magnetic quantum limit, which has so far been inaccessible in natural graphene. Molecular graphene provides a versatile means of synthesizing exotic topological electronic phases in condensed matter using tailored nanostructures.

The Dirac fermion has emerged as a common feature of new materials whose band structure and embedded spin degree of freedom are described by the relativistic Dirac equation[1]. In two dimensions, it has long been appreciated theoretically that the honeycomb lattice and mapping of the sublattice degree of freedom to a pseudospin is represented by the Dirac equation for electrons bound to the lattice, $H_G = \hbar\tilde{c}\boldsymbol{\sigma}\cdot\mathbf{k}$, where $\mathbf{k}$ is the vector momentum, $\boldsymbol{\sigma} = (\sigma_x, \sigma_y)$ and σ_i are the 2×2 Pauli spin matrices coupled to pseudospin, $\tilde{c}$ is the Dirac fermion velocity (the effective speed of light) and $\hbar$ is Planck's constant divided by 2π. The simplest model for this physics is captured in the two-site tight-binding band structure characterized by a hopping-matrix element, t, describing the bond strength between nearest-neighbour atoms separated by a distance a. Although this model is realized naturally in graphene, where carbon atoms comprise the honeycomb structure, it is more general and can describe any atoms in the same lattice, and even electrons alone, subject to the same symmetries but devoid of atomic 'containers'. However, tunable artificial Dirac fermions in honeycomb lattices have not been found in either atomic[3,4] or condensed-matter[13,14] systems.

In this work, we show that the synthesis and control of Dirac fermions in a general solid-state material is readily possible and can be interpreted in terms of simple ideas such as the decoration of crystal surfaces with atoms or molecules and periodic and aperiodic assembly, and by the application of familiar band structure models. In principle, any two-dimensional electron system (2DES) can be transformed into a host for Dirac fermions if it is patterned with a suitable periodic array of gates. In the case of top gates biased to a positive potential relative to a buried 2DES, a honeycomb arrangement of gates or dots[14] is necessary to induce electrons to form a graphene structure. The dual of this configuration can also be exploited: for negative potentials that deplete electrons under the gates, a triangular gate array leaves electrons in a honeycomb pattern and is described by the same Dirac Hamiltonian. Recently we showed how single atoms can function as atomic-size gates of a 2DES at noble metal surfaces[15] and how simple molecules such as CO function as repulsive potentials for surface electrons when shaped into open[5] and closed[16] quantum structures. Here we use individual CO molecules arranged molecule by molecule on a Cu(111) surface as a tunable gate array to transform a 2DES passing through these lattices into Dirac fermions, whence the term 'molecular graphene'. The specific potentials established induce these quasi-particles to condense into various topological phases. The resulting nanostructures need not even be periodic. In fact, control over every lattice position and potential in the artificial materials we construct provides unprecedented control of the spatial texture of the hopping parameter, ultimately allowing observation of electronic ordering into ground states rarely encountered in natural systems. (See Supplementary Fig. 1 for a summary.)

The starting point of our experiment is the nearly free 2DES on Cu(111), which is characterized by very long coherence lengths (>1,000 Å near the Fermi energy, E_F, where the sample bias is $V = E/e = 0$ and e is the electron charge), a band edge at $E_0 = -0.45$ eV and an effective mass of $m^* = 0.38m_e$, where m_e is the electron mass. For $E < 0.5$ eV, the dispersion relation is parabolic and the Fermi velocity is $v_F = 6.45 \times 10^5$ m s^{-1}. Carbon monoxide molecules are adsorbed on clean Cu(111) and a lattice is assembled by positioning the molecules individually using the tip of a scanning tunnelling microscope (Fig. 1a and Supplementary Video 1). All experiments were performed at a temperature of 4.2 K. By applying a periodic potential at the surface, we can embed a topological singularity into the energy bands, thus forming a Dirac point and producing linear carrier dispersion. In this work, we made molecular graphene consisting of ~100–1,000 molecules. For large lattices, the numbers of equivalent C sites and C–C bonds are respectively almost two and three times the number of assembled molecules.

[1]Department of Physics, Stanford University, Stanford, California 94305, USA. [2]Stanford Institute for Materials and Energy Sciences, SLAC National Accelerator Laboratory, Menlo Park, California 94025, USA. [3]Department of Electrical Engineering, Stanford University, Stanford, California 94305, USA. [4]Department of Applied Physics, Stanford University, Stanford, California 94305, USA. [5]Instituto de Ciencia de Materiales de Madrid, CSIC, Cantoblanco, E-28049 Madrid, Spain.
*These authors contributed equally to this work.

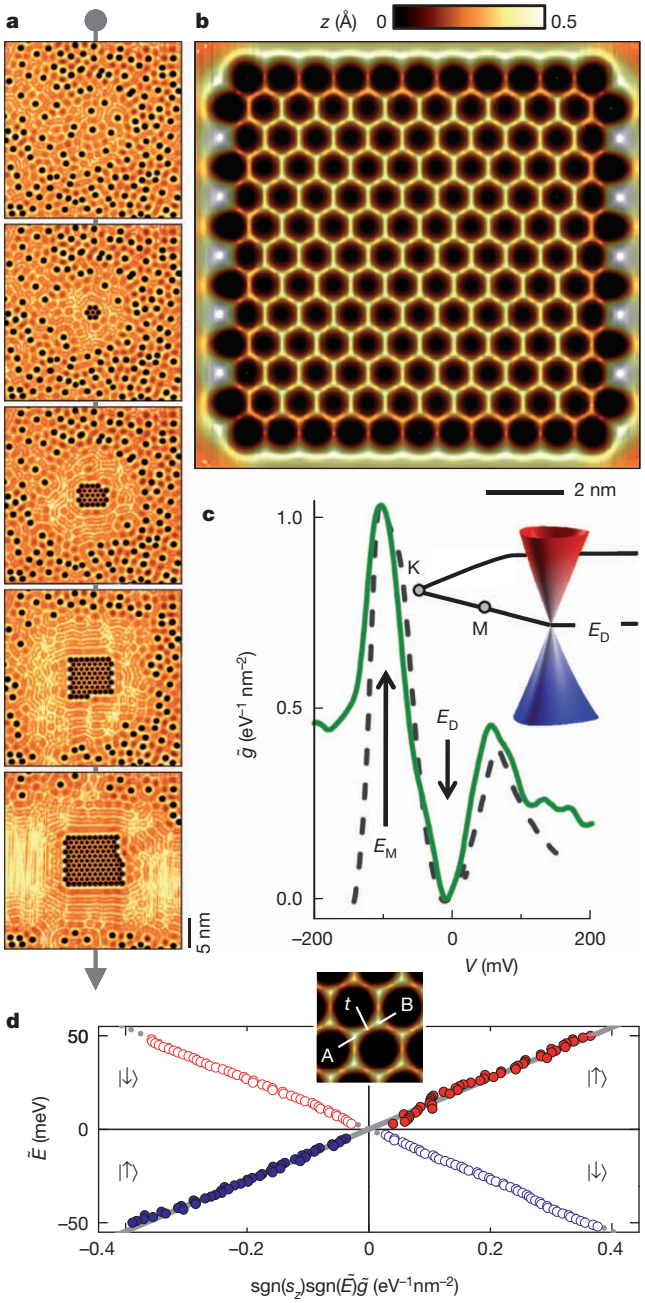

Figure 1 | Dirac fermions in molecular graphene. **a**, Sequence of constant-current topographs during the assembly of a molecular graphene lattice ($V = 10$ mV, $I = 1$ nA). **b**, Topograph of a molecular graphene lattice composed of 149 CO molecules (lattice constant, $d = 8.8$ Å). **c**, Spatially averaged, normalized differential conductance spectrum, $\tilde{g}(V)$ (solid line), measured on the top sites near the centre of quasi-neutral molecular graphene ($d = 19.2$ Å), accompanied by a tight-binding DOS fit (dashed line) with hopping parameters $t = 90$ meV and $t' = 16$ meV. Inset, resulting Dirac cone realized in reciprocal space (corresponding to fit parameters). The tight-binding spectrum is calculated by finding energy eigenvalues of a finite graphene lattice with Lorentzian basis functions (to model the finite lifetime due to scattering to bulk states and coupling to the two-dimensional continuum at the graphene edges, we used an electron self-energy $\Sigma = \Gamma/2$, where the linewidth is $\Gamma = 40$ meV from observed broadening of states near E_F). **d**, Linearly dispersing quasi-particles revealed by the conductance spectra $\tilde{g}(\tilde{E},r)$, plotted individually for sublattice A (filled circles: pseudospin $s_z = +1/2$, $|\uparrow\rangle$) and sublattice B (open circles: pseudospin $s_z = -1/2$, $|\downarrow\rangle$), measured at locations r illustrated in the inset. Points for $|\tilde{E}| \lesssim eV_{rms}$, where V_{rms} is the modulation voltage, are excluded from this plot because this instrumental broadening prohibits their accurate measurement.

A completed 'flake' of molecular graphene is shown in topographic form in Fig. 1b, demonstrating a perfect internal honeycomb lattice and discernable edge effects at the termination boundaries. The spectrum shown in Fig. 1c was measured at the lattice C sites near the centre of a lattice built using 271 CO molecules separated by a distance $d = \sqrt{3}a = 19.23$ Å. The spectra in all the figures show surface-state conductance, $\tilde{g}(E,r)$, where r denotes the measurement position. (Henceforth, 'tilde' quantities refer to continuum properties of the Dirac fermions.) These spectra are measured by taking the ratio, g_R, between the measured differential tunnelling conductance and the spatially averaged value acquired on clean Cu(111) (Supplementary Fig. 2). This normalization removes the featureless slope present in the bare Cu spectrum and cancels the effect of possible energy-dependent tunnelling matrix elements that may vary between different microscope tips. The jump in differential conductance at the two-dimensional band edge, $g_{2D} = m^*/\pi\hbar^2 = 1.585\,\mathrm{eV}^{-1}\,\mathrm{nm}^{-2}$, additionally provides a quantitative calibration of the surface density of states (DOS) and is used to scale g_R to meaningful units (Supplementary Information).

The edge of the gap at the M point in momentum space (Fig. 1c) is marked by the peak in conductance at $E_M = -104$ meV. The Dirac

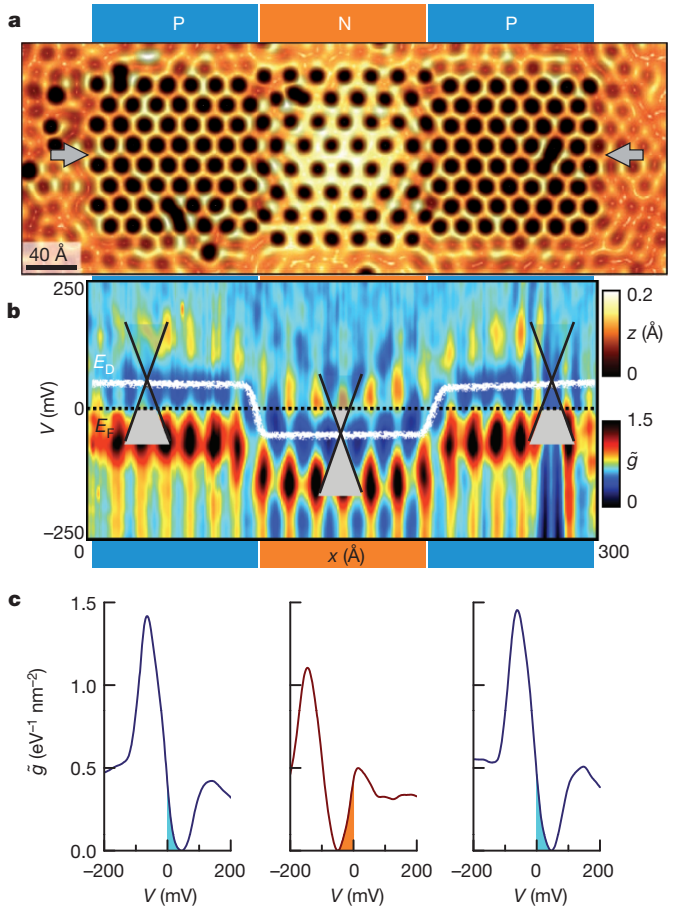

Figure 2 | Dirac point engineering in a p–n–p junction. Spectroscopic measurements made from a p–n–p lattice with alternating lattice spacings: d changes abruptly from 17.8 to 20.4 Å and then back again. **a**, Topograph of the p–n–p lattice. The conductance spectra were measured across the centre line marked by the grey arrows. **b**, Intensity colour plot of the conductance spectra $\tilde{g}(V,x)$, where x denotes the distance along the centre line. The white line is the locus of minima (the Dirac points (E_D)) in the conductance spectra. The dashed line marks the Fermi energy (E_F). Illustrative Dirac cones are superimposed to show the effective doping of each region. **c**, Spatially averaged, normalized conductance spectra measured along the centre line (marked by arrows in **a**). The first spectrum (blue, left) was measured in the left-hand, p-type, region ($d = 17.8$ Å), the second (orange, centre) was measured in the central, n-type, region ($d = 20.4$ Å) and the third (blue, right) was measured in the right-hand, p-type, region ($d = 17.8$ Å).

point is marked by the conductance minimum at $E_D = -5$ meV. Although the 2DES is normally decoupled from the bulk electrons for pure Cu, the presence of the molecules allows finite scattering and hence adds to the lifetime broadening evident in $\tilde{g}$. In a direct comparison with graphene tight binding, the nearest-neighbour hopping energy scale can be read from the data in Fig. 1c as $t \approx E_M - E_D = 99$ meV. The corresponding Dirac velocity is $\tilde{c} = 3ta/2\hbar = (2.5 \pm 0.2) \times 10^5$ m s^{-1}. The distinctive graphene spectral signature observed (Fig. 1c) can be contrasted with the electronic structure of the honeycomb lattice inverse, which is a (non-Dirac) triangular electron lattice (Supplementary Fig. 3). The successful match to tight-binding theory in both cases demonstrates the promise of these techniques for realizing many other lattice types.

A complementary model uses the nearly free electron model and 'muffin-tin' potential[17] to extract the properties of the emergent Dirac fermions. This approach (Supplementary Information) yields the position of the Dirac point, centred at the K points of the supercell Brillouin zone. For a wide range of Fourier coefficients of the superlattice potential, the nearly free electron model predicts that $t = 4\sqrt{3}\pi\hbar^2/27m^*a^2 = E_M - E_D = 118$ meV and that $\tilde{c} = 2\pi\hbar/3\sqrt{3}m^*a = (3.3 \pm 0.2) \times 10^5$ m s^{-1}, in good agreement with the parameters deduced from the tight-binding model.

The pseudospin structure of the Dirac point can be probed by directly tunnelling into the A and B sublattice sites[17]. Figure 1d shows plots of $\tilde{E} = E - E_D$ versus $\tilde{g}$ for the two sublattices, with a sign modification depending on which sublattice is probed. This method interrogates the underlying wavefunction overlap with each pseudospin s_z, and reveals the underlying massless Dirac fermion structure in the assembled nanomaterial. The slopes of the observed linearly vanishing DOS yield $\tilde{c} = (3.1 \pm 0.2) \times 10^5$ m s^{-1}. This and the above values for $\tilde{c}$ are in reasonable agreement and also match an expected theoretical value of $\tilde{c} \approx v_F/2 \approx 3.2 \times 10^5$ m s^{-1} for the nearly free electron model[17]. Just as in real graphene[1], an electron–hole asymmetry is observed in our molecular graphene (Fig. 1c). This asymmetry is due to a finite second-nearest-neighbour hopping-matrix element, t'. A full tight-binding fit to the experiment (Fig. 1c) yields $t = 90$ meV and $t' = 16$ meV. These values agree well with the potential model (Supplementary Information). The resulting Dirac cone centred at each K point in reciprocal space is plotted in Fig. 1c (inset).

Although E_F is fixed for the underlying 2DES and cannot be changed by conventional electrostatic gating, we are able to modify the lattice parameters to change the electron count per superlattice unit cell and thus control the graphene doping level. Making these changes on the atomic scale permits a change in the Dirac fermion carrier concentration over very short distances. To demonstrate this idea, we built molecular graphene with alternating CO lattice spacings, starting with $d = 17.8$ Å and abruptly changing to 20.4 Å and then back to 17.8 Å (Fig. 2). In the lattice with the smaller spacing, the Dirac point is located 46 meV above E_F, leading to a hole-doped (p-type) lattice with a carrier density of 1.41×10^{12} cm^{-2} (Fig. 2a). The lattice with the larger spacing is electron doped (n-type), with the Dirac point located 49 meV below E_F and a carrier density of 1.23×10^{12} cm^{-2} (Fig. 2c). We measure the

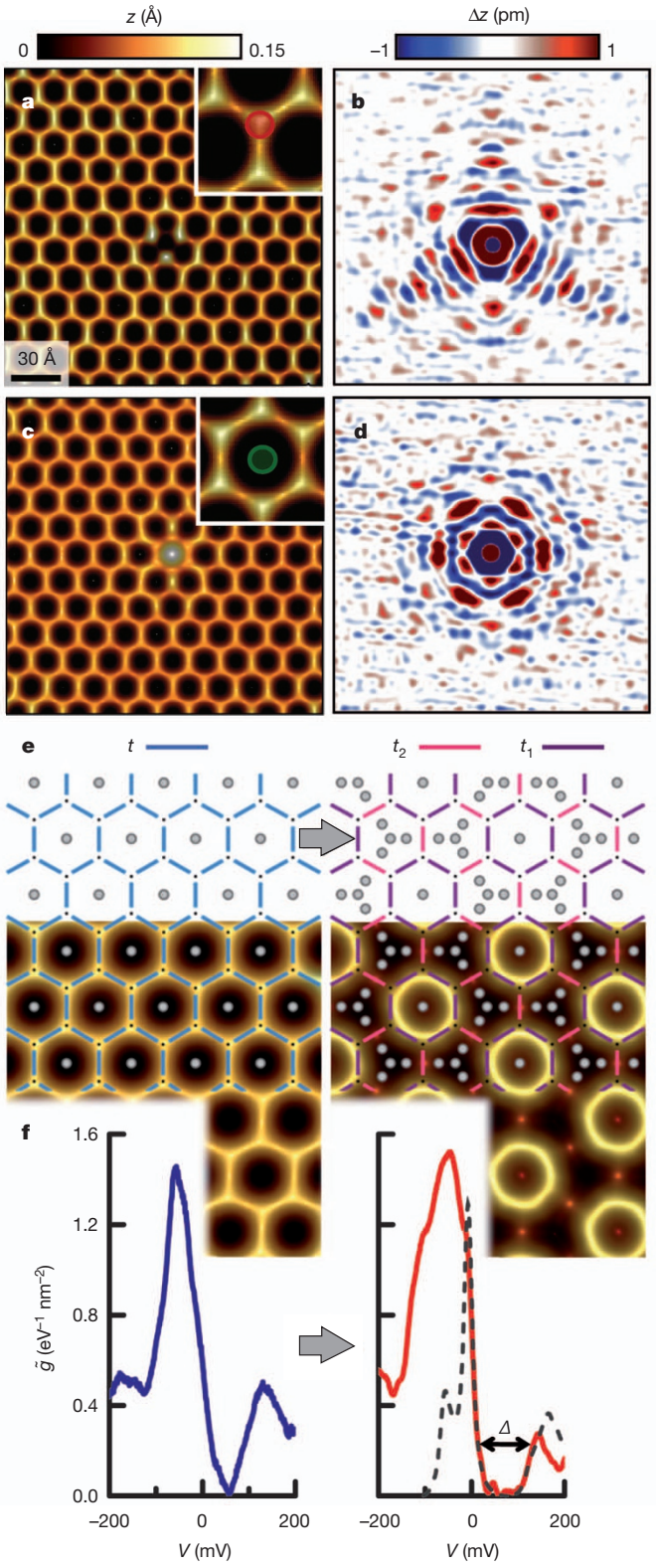

Figure 3 | Charge- and bond-density waves in molecular graphene. **a**, Topographic image of quasi-neutral molecular graphene ($d = 19.2$ Å), with an additional CO molecule at the top site (location indicated in inset). **b**, Impurity scattering quasi-particle interference mapped through the subtraction of two topographs ($V = 10$ mV, $I = 1$ nA) measured in identical fields of view and distinguished only by the presence of the extra CO molecule at the top site. **c**, Topograph of quasi-neutral molecular graphene ($d = 19.2$ Å), with the central CO molecule removed from the empty site (location indicated in inset). **d**, Corresponding difference map of two topographs measured as above, revealing quasi-particle interference of higher symmetry. **e**, Left: schematic of a pure molecular graphene lattice (grey circles denote CO molecule positions, small black dots are C sites, blue lines represent uniform hopping parameter t). At bottom, the schematic is overlaid with a topograph of the corresponding experimental lattice ($d = 17.8$ Å). Right: schematic of the modifications to pure molecular graphene to obtain a Kekulé hopping texture. The addition of extra CO molecules (grey circles) splits the nearest-neighbour hopping parameter into two different values (t_1 in purple and t_2 in pink, $t_1 > t_2$), as illustrated. At bottom, the transformation schematic is overlaid with measured topography from experiment after molecular manipulation ($d = 19.2$ Å). **f**, Conductance spectra measured in pure molecular graphene (blue) and in the graphene lattice after the Kekulé texturing (red). The spectra display the opening of a gap, Δ, at the Dirac point. Dashed curve, tight-binding fit calculated with $t_1 = 2t_2$. The small difference in d compensates for the change in chemical potential introduced by the extra CO molecules.

surface spectrum ($\tilde{g}$) across the lattice along the line indicated (Fig. 2a, b, arrows), crossing all regions. Because there are no charging effects, the interface between the p- and n-type regions is very narrow: it is about 20 Å wide (Fig. 2b). The extremely short transition between the p- and n-type regions makes this device a suitable candidate in which to study phenomena such as the Klein paradox[18] or to create a Veselago lens[19].

Using atomic manipulation, we created both pseudospin-conserving and pseudospin-breaking local disturbances further to reveal the Dirac nature of our system. We started with quasi-neutral molecular graphene with E_D near E_F (271 CO molecules, $d = 19.2$ Å) and tested two symmetries (a C-site defect (Fig. 3a), which locally imbalances the sublattices, and an empty-site vacancy (Fig. 3c), which locally preserves sublattice symmetry); these two structures are topologically distinct because their potentials correspond respectively to a local vector potential and a local scalar potential coupling to pseudospin. By subtracting two low-bias scanning tunnelling microscope topographs, one with the impurity and the other without it, and both locked to exactly the same area and using identical measurement parameters, we obtain detailed pseudospin maps resulting from the tiny DOS perturbations caused by quantum interference. The distinct patterns observed have the three-fold symmetry (Fig. 3b) predicted for single impurities in graphene that disrupt the Berry phase[20], rather than the full six-fold symmetry of a scalar perturbation, which conserves pseudospin[21–23] (Fig. 3d).

Topological changes fundamentally alter the lattice symmetry and are the key to unlocking physical phenomena such as electron fractionalization[6–8,10–12,22]. In graphene, one of the simplest (yet unrealized) deformations is the Kekulé distortion rooted in the historical interpretation of benzene. This distortion breaks the bond symmetry of graphene by forming two hopping elements, t_1 and t_2, in the pattern shown in Fig. 3e. We produce this distortion using a special 'Mercedes' arrangement of CO molecules in the honeycomb empty sites. This has the effect of modulating the strength of every other C–C bond along the perimeter of each cell. Such a distortion adds an off-diagonal term to the Hamiltonian[11], such that

$$H_G = \begin{pmatrix} \hbar\tilde{c}\boldsymbol{\sigma}\bullet\mathbf{k} & \Delta I_{2\times 2} \\ \Delta^* I_{2\times 2} & -\hbar\tilde{c}\boldsymbol{\sigma}\bullet\mathbf{k} \end{pmatrix}$$

where $I_{2\times 2}$ is the two-by-two identity matrix and an asterisk denotes complex conjugate. This distortion is predicted to open an energy gap, Δ, even if the underlying sublattice symmetry is not broken; notably, this effect has never been observed. Figure 3f proves that the Kekulé distortion works as theoretically predicted, creating massive Dirac fermions out of the massless Dirac fermions in the pristine lattice. From fits to theory, the mass of the emergent fermions is $m_D = 0.1 \pm 0.02\, m_e$. The Kekulé ground state[10–12,24,25] has an intriguing mapping to a superconducting topological surface state[26], after pseudospin is mapped to spin and the valley degree of freedom to an isospin, equivalent to attaching a scalar gauge field that produces a Dirac fermion mass. This scalar gauge field is manifest in the bond-density wave mosaic structure visible in Fig. 3e. The transition from massless to massive Dirac fermions has been theoretically cast as a quantum phase transition[3,11]; the molecular graphene system provides an experimental test bed of these ideas starting with the spontaneous generation of mass observed here.

The chiral character of the electronic charge in graphene is due to the pseudospin associated with the symmetry between the two triangular sublattices that form the honeycomb lattice. It has been proposed that by breaking this sublattice symmetry through strain, it is possible to generate a pseudomagnetic field and therefore obtain Landau levels and quantum Hall phases without breaking time reversal symmetry. The effect of strain has recently been observed in graphene nanobubbles[27], but tunable molecular graphene offers much more precise and *in situ* control over internal gauge fields. The strain field displacements in polar coordinates (r and θ) suggested[9] to generate a constant field are $(u_r, u_\theta) = (qr^2\sin(3\theta), qr^2\cos(3\theta))$, where q is a parameter denoting the strength of the strain. In our final experiment, we applied this strain field to molecular graphene by means of atomic manipulation.

Topographs for successively strained graphene are shown in Fig. 4a. The value of the pseudomagnetic field can be estimated as $\tilde{B} = 8\beta\hbar q/ea = 16\pi q\hbar/3de$, where $\beta = -\partial\ln(t)/\partial\ln(a) \approx 2$ (Supplementary Information). We study strain values up to $q = 10^{-3}$ Å^{-1}, which is

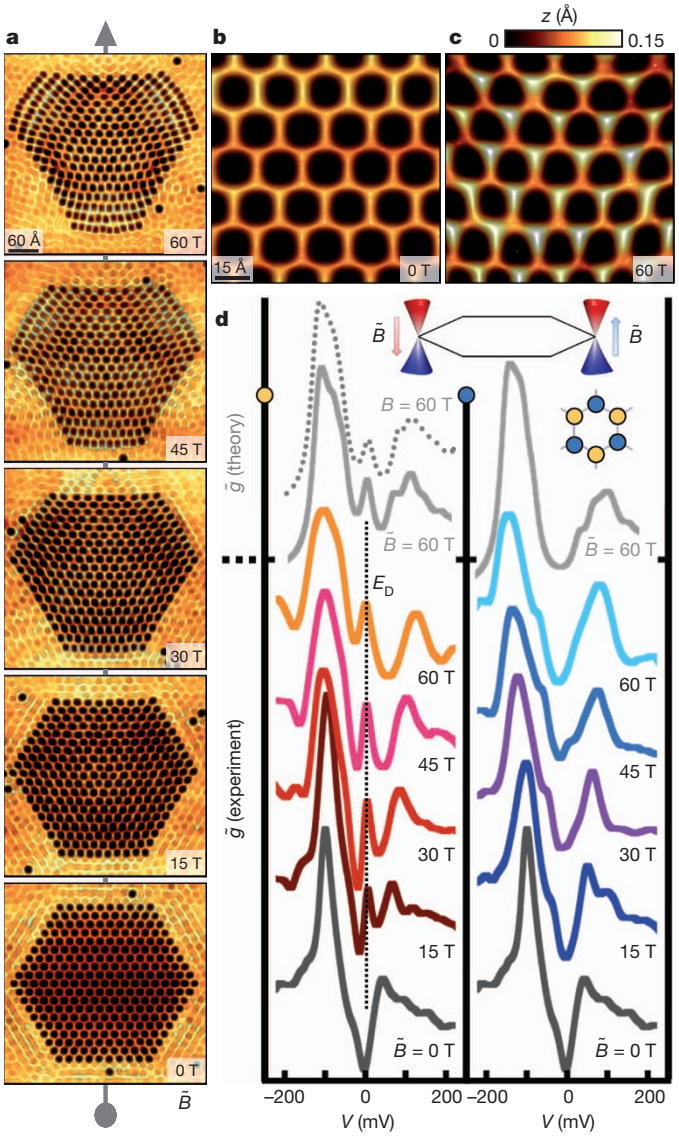

Figure 4 | Landau quantization and topological zero modes in a tunable pseudomagnetic field. **a**, Sequence of topographs of molecular graphene lattices with increasing values of triaxial strain. The position of each CO molecule was determined by the dislocation vector defined in the main text. From bottom to top, $q = 0$, 2.5×10^{-4}, 5×10^{-4}, 7.5×10^{-4} and 10^{-3} Å^{-1}. The corresponding values of the constant pseudomagnetic field are $\tilde{B} = 0$, 15, 30, 45 and 60 T (felt in opposite directions by the two graphene valleys; see **d**, top inset). **b**, Topograph at the centre of the lattice without strain distortion ($q = 0$ Å^{-1}), showing the unbroken symmetry between each sublattice (pseudospin) of the honeycomb. **c**, Topograph at the centre of the lattice with strain distortion ($q = 10^{-3}$ Å^{-1}), showing the broken symmetry between each sublattice (one bright and one dark) as a result of the localization of the zero Landau level on half of the sample (bright sublattice). **d**, Left: normalized conductance spectra measured on sublattice A (brighter top sites in **c** and orange circles in inset schematic) for successive values of strain. The spectra were measured near the centres of the lattices shown in **a**. Right: spectra measured on sublattice B (darker top sites in **c** and blue circles in inset schematic) for the same successive values of strain, showing the opening of a Landau gap. Grey solid curves are tight-binding fits of strained finite lattices to the experiment. The grey dotted curve shows a tight-binding calculation in a real magnetic field, $B = 60$ T, for an unstrained lattice of the same dimensions and hopping parameters.

equivalent to a pseudomagnetic field of $\tilde{B} \approx 60$ T, corresponding now to a vector gauge field dressing the Dirac fermions (the applied triaxial strain can be contrasted with uniaxial strain (Supplementary Fig. 4), which is devoid of gauge fields). The breaking of the pseudospin symmetry of the Dirac point can be probed by direct tunnelling into the individual sublattice sites. Once the strain is applied, the symmetry breaking between the two sublattices is discernible in the topographs (Fig. 4b, c) and can be noticed in the spectra (Fig. 4d). In the 'bright' sublattice (A), a well-defined zero-bias state—the zero Landau level—forms and gains prominence with increasing strain. In the 'dark' sublattice (B), the spectra are characterized by a reduction in the conductance at zero bias with strain—the formation of a Landau gap—visible through the transformation of typical V-shaped spectra into U-shaped contours.

The presence of a zeroth Landau level at the Dirac point is one of the hallmarks of the quantum Hall effect with Dirac fermions. The low Fermi velocity here means that even a small strain can push the first excited Landau level beyond the linear regime in the band structure, towards or beyond the edge of the M-point gap. We estimate that for our lowest value of strain ($q = 0.25 \times 10^{-3}$ Å^{-1}), $\tilde{B} \approx 15$ T and the $n = 1$ Landau level therefore lies at 33 mV. The registry of the CO molecules to the surface Cu atoms quantizes the allowed lattice sizes and hinders the formation of lattices with smaller strains. Nevertheless, a complete quantitative model of our finite system shows that it behaves as a graphene quantum dot in a real magnetic field, B, when these strain fields are applied (in Fig. 4d, tight-binding fits for finite strain and zero B and for zero strain and high B both provide excellent reproductions of the observations).

Owing to the large strains applied, the particular topological state observed here is an ultraquantized ground state: only the zeroth Landau level is present and fractionally occupied by Dirac fermions. Such a state is unprecedented in normal graphene owing to the larger energy scales and, hence, very large magnetic fields necessary to study it. The pseudospin symmetry breaking observed is connected with the fundamental index theorem, which predicts the same topological phase for Dirac fermions on a lattice[28] as is observed here. In this phase, the electrons in the zero mode form a peculiar condensate in which they become completely delocalized over the sample but remain alternately localized and antilocalized in the pseudospin projection[29] (Supplementary Information). The image in Fig. 4c provides a snapshot of this intriguing phase in real space.

The study of artificial lattices may lead to technological applications, but they also provide a new level of control over Dirac fermions and allow experimental access to a set of phenomena that has hitherto been considered only theoretically. The introduction of tunable interactions between the electrons could lead to the formation of spin liquids in graphene, and the addition of spin–orbit coupling could lead to a quantum spin Hall effect. The time-reversal-invariant quantum Hall state observed here already has a direct connection to the two-dimensional topological insulator[9]. In future, such topological phases may be produced even more easily by extending our manipulation techniques to self-assembly methods[30], which naturally generate long-range periodic potentials on decorated surfaces.

Received 8 July 2011; accepted 9 February 2012.

1. Castro Neto, A., Guinea, F., Peres, N., Novoselov, K. & Geim, A. The electronic properties of graphene. *Rev. Mod. Phys.* **81,** 109–162 (2009).
2. Bloch, I. Ultracold quantum gases in optical lattices. *Nature Phys.* **1,** 23–30 (2005).
3. Zhu, S.-L., Wang, B. & Duan, L.-M. Simulation and detection of Dirac fermions with cold atoms in an optical lattice. *Phys. Rev. Lett.* **98,** 260402 (2007).
4. Wunsch, B., Guinea, F. & Sols, F. Dirac-point engineering and topological phase transitions in honeycomb optical lattices. *N. J. Phys.* **10,** 103027 (2008).
5. Moon, C. R., Mattos, L. S., Foster, B. K., Zeltzer, G. & Manoharan, H. C. Quantum holographic encoding in a two-dimensional electron gas. *Nature Nanotechnol.* **4,** 167–172 (2009).
6. Chamon, C. *et al.* Irrational versus rational charge and statistics in two-dimensional quantum systems. *Phys. Rev. Lett.* **100,** 110405 (2008).
7. Seradjeh, B., Weeks, C. & Franz, M. Fractionalization in a square-lattice model with time-reversal symmetry. *Phys. Rev. B* **77,** 033104 (2008).
8. Ryu, S., Mudry, C., Hou, C.-Y. & Chamon, C. Masses in graphenelike two-dimensional electronic systems: topological defects in order parameters and their fractional exchange statistics. *Phys. Rev. B* **80,** 205319 (2009).
9. Guinea, F., Katsnelson, M. I. & Geim, A. K. Energy gaps and a zero-field quantum Hall effect in graphene by strain engineering. *Nature Phys.* **6,** 30–33 (2010).
10. Jackiw, R. Fractional charge from topology in polyacetylene and graphene. *AIP Conf. Proc.* **939,** 341–350 (2007).
11. Hou, C.-Y., Chamon, C. & Mudry, C. Electron fractionalization in two-dimensional graphenelike structures. *Phys. Rev. Lett.* **98,** 186809 (2007).
12. Seradjeh, B. & Franz, M. Fractional statistics of topological defects in graphene and related structures. *Phys. Rev. Lett.* **101,** 146401 (2008).
13. Cahangirov, S., Topsakal, M., Aktürk, E., Şahin, H. & Ciraci, S. Two- and one-dimensional honeycomb structures of silicon and germanium. *Phys. Rev. Lett.* **102,** 236804 (2009).
14. Singha, A. *et al.* Two-dimensional Mott-Hubbard electrons in an artificial honeycomb lattice. *Science* **332,** 1176–1179 (2011).
15. Moon, C. R., Lutz, C. P. & Manoharan, H. C. Single-atom gating of quantum-state superpositions. *Nature Phys.* **4,** 454–458 (2008).
16. Moon, C. R. *et al.* Quantum phase extraction in isospectral electronic nanostructures. *Science* **319,** 782–787 (2008).
17. Park, C.-H. & Louie, S. G. Making massless Dirac fermions from a patterned two-dimensional electron gas. *Nano Lett.* **9,** 1793–1797 (2009).
18. Katsnelson, M., Novoselov, K. & Geim, A. Chiral tunnelling and the Klein paradox in graphene. *Nature Phys.* **2,** 620–625 (2006).
19. Cheianov, V., Fal'ko, V. & Altshuler, B. The focusing of electron flow and a Veselago lens in graphene p-n junctions. *Science* **315,** 1252–1255 (2007).
20. Wehling, T. O. *et al.* Theory of Fano resonances in graphene: the influence of orbital and structural symmetries on STM spectra. *Phys. Rev. B* **81,** 085413 (2010).
21. Wehling, T. O. *et al.* Local electronic signatures of impurity states in graphene. *Phys. Rev. B* **75,** 125425 (2007).
22. Guinea, F., Katsnelson, M. & Vozmediano, M. Midgap states and charge inhomogeneities in corrugated graphene. *Phys. Rev. B* **77,** 075422 (2008).
23. Bena, C. & Kivelson, S. A. Quasiparticle scattering and local density of states in graphite. *Phys. Rev. B* **72,** 125432 (2005).
24. Martin, I., Blanter, Y. & Morpurgo, A. Topological confinement in bilayer graphene. *Phys. Rev. Lett.* **100,** 036804 (2008).
25. Nomura, K., Koshino, M. & Ryu, S. Topological delocalization of two-dimensional massless Dirac fermions. *Phys. Rev. Lett.* **99,** 146806 (2007).
26. Roy, B. & Herbut, I. Unconventional superconductivity on honeycomb lattice: theory of Kekule order parameter. *Phys. Rev. B* **82,** 035429 (2010).
27. Levy, N. *et al.* Strain-induced pseudo-magnetic fields greater than 300 Tesla in graphene nanobubbles. *Science* **329,** 544–547 (2010).
28. Kailasvuori, J. Pedestrian index theorem à la Aharonov-Casher for bulk threshold modes in corrugated multilayer graphene. *Europhys. Lett.* **87,** 47008 (2009).
29. Herbut, I. Pseudomagnetic catalysis of the time-reversal symmetry breaking in graphene. *Phys. Rev. B* **78,** 205433 (2008).
30. Lobo-Checa, J. *et al.* Band formation from coupled quantum dots formed by a nanoporous network on a copper surface. *Science* **325,** 300–303 (2009).

Supplementary Information is linked to the online version of the paper at www.nature.com/nature.

Acknowledgements This work was supported by the US Department of Energy, Office of Basic Energy Sciences, Division of Materials Sciences and Engineering, under contract DE-AC02-76SF00515. F.G. acknowledges financial support from MICINN (Spain) through grants FIS2008-00124 and CONSOLIDER CSD2007-00010, and calculations supported by the US National Science Foundation. We thank C.-H. Park, I. Martin, A. Balatsky, T. Wehling, A. Akhmerov, E. Heller and A. Fetter for discussions.

Author Contributions K.K.G., W.M. and W.K. designed and performed experiments, analysed data and wrote the manuscript. F.G. provided the theoretical analysis. H.C.M. directed the project and wrote the manuscript.

Author Information Reprints and permissions information is available at www.nature.com/reprints. The authors declare no competing financial interests. Readers are welcome to comment on the online version of this article at www.nature.com/nature. Correspondence and requests for materials should be addressed to H.C.M. (manoharan@stanford.edu).